International Conference on. Quenching and Distortion Engineering 2018,
November 27-29, 2018, Nagoya, Japan (Manuscript) Arimotech Report: www.arimotech.com

Learning about Mechanisms of Distortion and Residual Stress Due to Heat Treatment by Simulated-Strain Based Approach

Kyozo Arimoto [1, a *]

[1] Arimotech Ltd., Osaka, Japan.

[a] kyozo_arimoto@arimotech.com

Keywords: Distortion, residual stress, heat treatment simulation, learning.

Abstract. Distortion and residual stress in steel parts due to heat treatment affect directly performance and life of assembled products. A trial and error method has been used traditionally to solve the problems, which requires a lot of time and cost. In the 1970s, heat treatment simulation realized based on theoretical studies for predicting a variety of quantities, temperature, volume fraction of metallic phase, stress, strains, and so on, during the processes. Into the 2000s, an approach was established to explain the origin of distortion and residual stress based on the simulated results, especially various kinds of strains, which is called as the simulated-strain based approach here. There are several companies that are engaged in providing practical knowledge from experts to engineers on one-day courses in Japan. The author participates in the activity as a speaker to give a talk on mechanism of distortion and residual stress due to heat treatment. His talk provides an overview of distortion, stress-strains, fractures, and the theory of heat treatment simulation by an organized way. Then the simulated-strain based approach are presented by using applications to simple-shaped parts such as long objects, cylinders, and rings, which were normal quenched, carburizing quenched, induction hardened, and nitrided. Additionally the origin of quench cracking is explained in his presentation. This paper describes selected learning materials in the author's one-day course to clarify how heat treatment engineers should learn about mechanisms of distortion and residual stress.

Introduction

In recent years, reduction of distortion due to heat treatment has been required strictly because of higher precision in enhanced parts. Usually, this target has been achieved by trial and error, which takes a lot of time and cost. Explanations of the causes of distortion for a fundamental solution have been mainly attempted based on experimental and theoretical studies with a simple shaped test piece.

In the 1970s, theoretical studies on heat treatment distortion and residual stress produced simulation software. The codes predict distortion, stress, and various strains such as elastic, thermal, phase transformation, plastic, and creep strains in parts during processes. Based on distributions of these simulated strains, the author devised a procedure to explain reasons of distortion and stress generation in the 2000s, which is called as the simulated-strain based approach [1]. It is meaningful for heat treatment engineers to know the approach for solving their immediate problems.

One-day courses to educate engineers in various fields by specific experts are organized by some private engineering education companies in Japan. The author participates in a course on mechanism of distortion and residual stress due to heat treatment for past 10 years. In general, heat treating engineers who majored in materials science and engineering do not have the opportunity to learn sufficiently about the stress and strain. On the other hand, even if they majored in mechanical engineering, they are hardly taught about distortion and residual stress due to heat treatment. After all, the author's course explains to them about essence of stress and strain by his original learning materials for intuitive understanding.

Subsequently, the author explains models of phase transformation, heat conduction, diffusion, stress/strain, etc., in heat treatment simulation. Then, he shows simulated results of simple shaped parts during normal quenching, carburizing quenching, induction hardening, nitriding, etc., and explains the origin of distortion and residual stress by the simulated-strain based approach.

This paper describes selected learning materials in the author's one-day course and suggests how heat treatment engineers should learn about the distortion and residual stress due to heat treatment.

Learning Materials for Intuitive Understanding of Stress-Strain Behavior

The author has developed learning materials for intuitive understanding of stress-strain in elastic-plastic material due to force and thermal expansion for the introduction part of his course [2]. Contents on the mechanics of material and the materials science have been merged for the materials.

Stress and Strain in Mechanics of Materials. Uniaxial stress and strain are defined using a round bar with length L, and elongation δ under tension load P in the textbook [3]. The bar made of homogeneous material is uniform throughout its volume, and the loads act through the centroids of the cross sections. That is, the uniaxial strain ε and the uniaxial stress σ are obtained by δ/L and P/A, respectively, where A is the cross-sectional area of the bar.

The author explains the mechanism of residual uniaxial strain generation in a tensile test piece by the stress-strain diagram in Fig. 1 [3]. When pulling the test piece, the uniaxial stress-strain condition moves from the stage O and passes through the stage A. When plastic phenomenon occurs with increasing load, the condition moves to a stage on the second straight line, and reaches the stage B. After unloading, the condition moves along line BC and attains the stage C.

The total strain corresponding to the line segment OB' is elastically recovered by the strain CB' and the strain OC remains as a permanent deformation. The segments CB', OC and OB' correspond to elastic strain ε^E, plastic strain ε^P and total strain ε, respectively, as shown in Fig. 1. Subsequently, the author describes the Hooke's law, $\sigma=E\varepsilon^E$, which is a relationship established between stress σ and elastic strain ε^E, where E is Young's modulus.

The author also states that the thermal strain ε^{TH} is expressed as $\alpha\Delta T$, where α is the coefficient of thermal expansion and ΔT is temperature change. The relation among elastic, thermal, plastic, and total strains is shown as follows:

$$\varepsilon = \varepsilon^E + \varepsilon^{TH} + \varepsilon^P . \qquad (1)$$

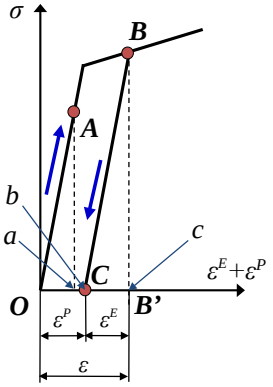

Fig. 1 Stress-strain diagram of elastic-plastic material

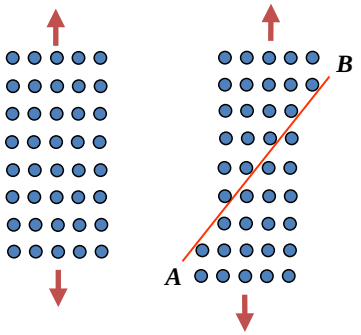

Fig. 2 Crystal structure model subjected to tension.

Stress and Strain in Materials of Science. The author introduces another idea on stress and strain in the field of materials science. Although plasticity is explained by the dislocation theory, Bowden and Taber [4] proposed Fig. 2 for plastic deformation, in which 40 atoms shown as filled circles are hypothetically taken out from a crystal structure and arranged on a plane.

Figure 2 (a) shows the model of the structure in elastic stage. When increasing load, a slip occurs along the line AB as shown in Fig. 2 (b), which is stated as plastic deformation hypothetically.

Conceptual Diagrams for Explaining Stress-Strain Generation. For understanding stress and strains, and also their relationship more intuitively, the author selected the elastic-plastic problem in a bar subjected to tensile load. He created Fig. 3 as a conceptual diagram using the 40 atom model with a unit length, which expresses the stages, initial: O, elastic deformed: A, elastic-plastic deformed: B, and unloaded: C, during tensile test in Fig. 1.

Interatomic distance changes due to elasticity are expressed in Fig. 3, instead of Fig. 2. In addition, amounts of strains and stress in the specific stages are shown near the 40 atom models of each stage.

The slip produced at the stage *B* explains visually the induction of permanent elongation *b* at the stage *C*.

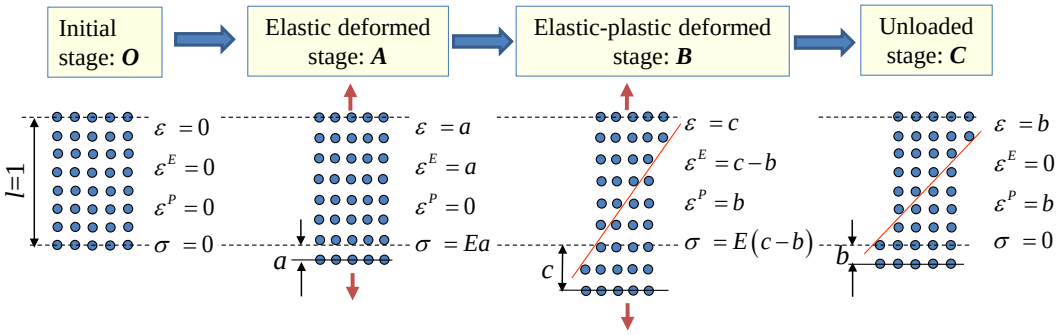

Fig. 3 Conceptual diagram of stress-strain stages in 40 atom model during tensile test

It is difficult to understand how thermal expansion affects elastic-plastic deformation in a solid. For solving this problem, the author uses a bar constrained at the both ends under a temperature cycle between the room temperature and a specific high temperature as shown in Fig. 4 (a). When approaching the high temperature, the bar enters the plastic region. After returning to the room temperature, constraint at the one of the ends is removed as shown in Fig. 4 (b). The stress-strain changes during the temperature cycle can be obtained using knowledge of mechanics of materials. As shown in Fig. 5, stress-strain state in the bar moves on the lines in the diagram through the specific stages, initial: *O*, elastic deformation: *A*, elastic-plastic deformation: *B*, initial temperature *C*: and unconstraint: *D*. When it is informed that thermal strains at stages *A* and *B* are *a* and *c*, respectively, the corresponded elastic-plastic strains $\varepsilon^E+\varepsilon^P$ at the same stages are *–a* and *–c*, respectively.

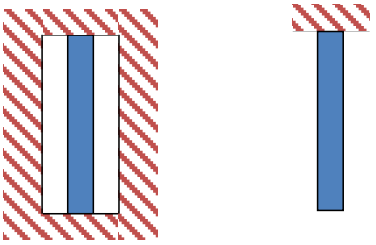

(a) Constraint (b) Unconstraint

Fig. 4 Shape and constraint condition of bar under temperature cycle

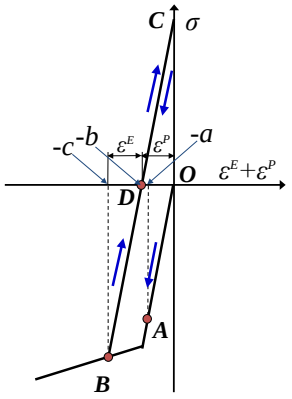

Fig. 5 Stress-Strain diagram of bar under temperature cycle

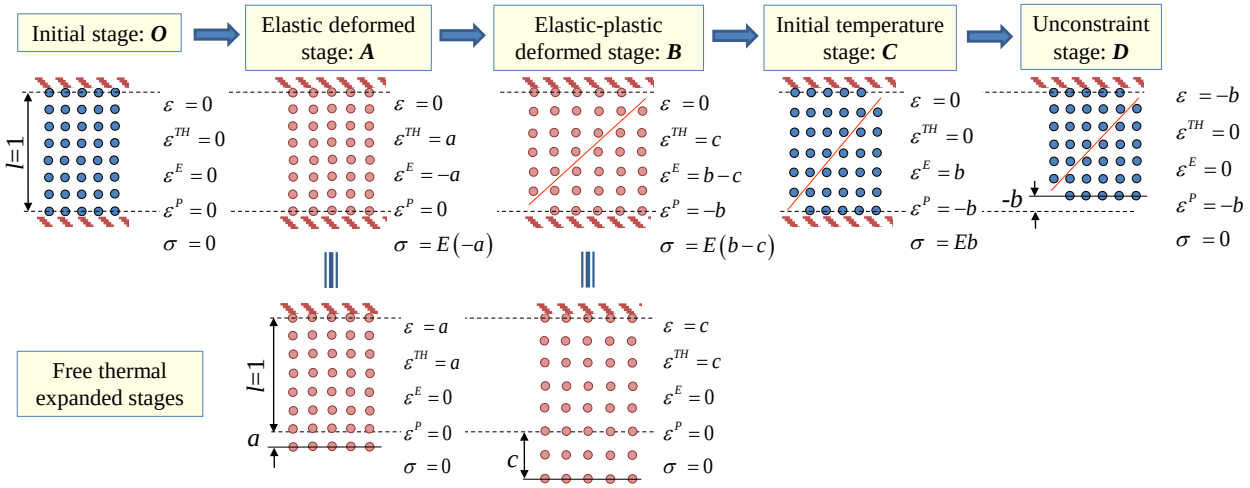

Fig. 6 Conceptual diagram of stress-strain states in 40 atom model during temperature cycle

Figure 6 shows the conceptual diagram created by expanding the concept of the Boden and Tabor's drawing to the condition under the temperature cycle. Free thermal expanded stages *A* and *B* are depicted for expressing the nature of crystal structure at the high temperature region. The condition of atoms during thermal expansion is expressed by expanding interatomic distance and changing color of atoms in the figure. Thermal expanded lengths are pushed back hypothetically to their original constraint condition so that real stages *A* and *B* are obtained. Residual stress at stage *C* and contraction at stage *D* in the model are explained visually by the slip which is induced at stage *B* due to the exceeded thermal strain. This conceptual diagram can be used to understand intuitively complicated stress-strain phenomena under temperature cycles.

Introduction to Simulated-Strain Based Approach for Understanding Springback Phenomenon

Springback [5,6] is meaningful as a previous step to explain about distortion during heat treatment using the simulated-strain based approach, although phase transformations are not included in the phenomenon. The author presents the springback in a pure bending beam shown in Fig. 7.

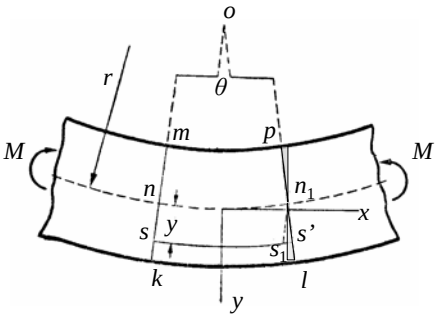

Fig. 7 Elastic-plastic bending beam

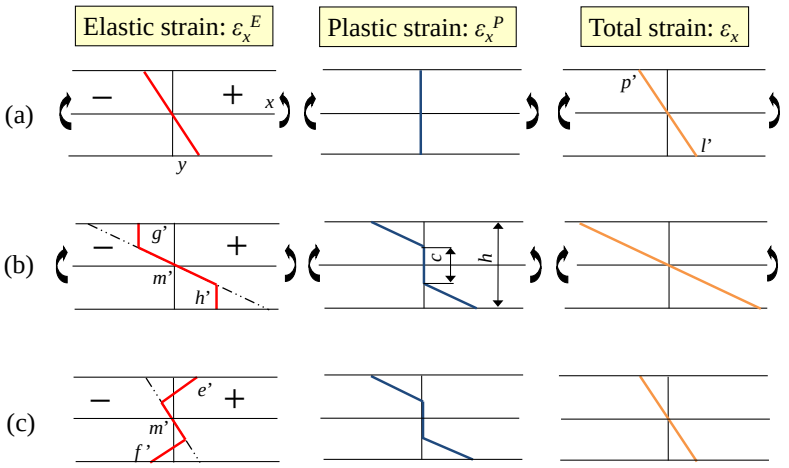

Fig. 8 Distribution of various strains in bending beam
(a) Elastic state (b) Before springback (c) After springback

The fiber length nn_1 along the neutral axis in Fig. 7 does not change in bending, while the length ss_1 at the distance y from the neutral axis changes to ss'. In the elastic region, the x component of elastic strain ε_x^E in the fiber is $s's_1/nn_1$, which is y/r ($=y\theta/r\theta$), where r is a curvature radius of the arc due to bending along the neutral axis. Stress in the x direction σ_x in the fiber is obtained by the Hooke's law as follows:

$$\sigma_x = E\varepsilon_x^E = E\frac{y}{r}. \tag{2}$$

Subsequently, the author presents Fig. 8 which shows distributions of various axial strains in the beam section schematically for the simulated-strain based approach. In the elastic state shown in Fig. 8 (a), elastic strain and total strain distributions are the same because of no plastic strain. It is obvious that distribution $p'l'$ in Fig. 8 (a) corresponds to the line pl in Fig. 7. The author emphasizes that the stress-strain behavior in the tensile test in Fig. 1 may occur in fibers in lower part of the beam section, while fibers in the upper part correspond to a compression test. Also, the 40 atom model shown in Fig. 3 can be used to explain the phenomena in the fiber microscopically,

Plastic strain is induced in the outermost fibers in the cross section and expanded to the inside with increasing the moment *M*. Figure 8 (b) shows the elastic-plastic bending stage before springback. Elastic strain distribution is derived corresponding to total strain in the elastic range *c*. Stress in the cross section can be obtained by multiplying the elastic strain by the Young's modulus in the elastic region, on the other hand, elastic strain and stress in the plastic region is a constant value, because material is assumed as an elastic perfectly plastic solid.

When the moment is unloaded, the spring back phenomenon occurs in the beam. The final curved shape corresponds to the total strain distribution shown in Fig. 8 (c), which has the smaller gradient than that in Fig. 8 (b). Assuming no plastic phenomenon occurs in the unloading process, the plastic

strain distribution in the stage (b) is directly brought to the stage (c). Then the elastic strain is generated based on the condition that this plastic strain and the linear total strain exist. Furthermore, the elastic strain distribution is subjected to the condition that the residual stress distribution after unloading is balanced in the cross section.

Figure 9 shows an example of a bending process for the 0.48 mm diameter copper wire using a printed template card [5,7]. The ends of the wire put on the card were pinched by fingers of both hands. Then a moment can be applied to the ends from the fingers to fit the wire shape for the specific arc on the card. Bending corresponding to the curvature radius 300 mm shows no permanent deformation in the wire after springback although the 150 mm radius bending showed residual curves. Assuming that the Young's modulus E of the copper is 127.5 GPa, 200 MPa is obtained as yield stress σ_Y from Eq. (2) when a curvature radius before springback r_{bsb} is 150 mm.

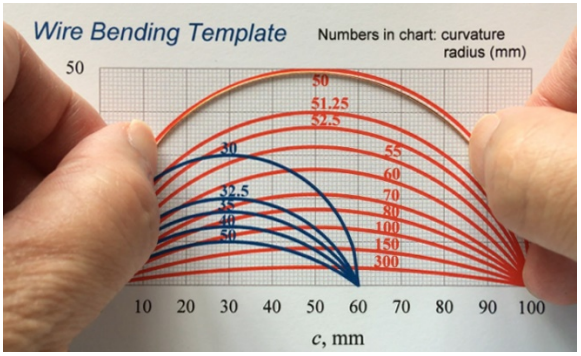

Fig. 9 Bending of copper wire by template [7]

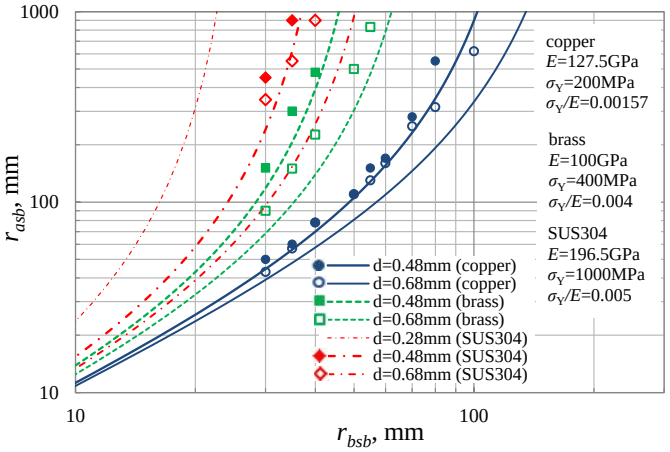

Fig. 10 Relation on r_{bsb} and r_{asb} in the different wires

Curvature radii after springback r_{asb} in copper, brass and austenitic stainless steel (SUS304) wires were measured with the bending template card and plotted as markers as shown in Fig. 10. The curves for each wire in the figure were drawn using Gardiner's formula [8] of metal wire winding under assuming the materials as elastic perfectly plastic solid, which obtains the change of coil curvature radius between before and after spring back as follows:

$$\Delta r = r_{asb} - r_{bsb} = r_{bsb}\left(\frac{2A}{\pi - 2A}\right), \tag{3}$$

where A is expressed as:

$$A = \sin^{-1} 2K + \frac{2}{3}K\sqrt{1-4K^2}\left(5-8K^2\right), \tag{4}$$

and K is a parameter including the ratio of yield stress σ_Y and Young's modulus E of the materials, and diameter of wire d as shown below:

$$K = \frac{r_{bsb}}{d}\frac{\sigma_Y}{E}. \tag{5}$$

The materials of wires shown in Fig. 10 do not have detailed information on their manufacturing processes including straightening and their chemical composition. Therefore, their yield stress and Young' modulus were confirmed by data in the materials education software CES EduPack [5,9].

Examples of Simulated-Strain Based Approach Applied to Heat Treated Parts

Outline of explanations in the author's course. The aim of the author's course is to explain about applications of the simulated-strain based approach to distortion, residual stress, and quench cracking due to heat treatment. Then, transformation and transformation plastic strains are added to the right side of Eq. (1). Furthermore, the author considers diffusion strains due to expansion caused by diffusion of interstitial carbon or nitrogen in carburizing and nitriding, and also creep strain due to heating.

Since stress and strains are tensor quantities, the relation on total strain ${}^t\varepsilon_{ij}$ and various strains obtained from simulation at time *t* in practical parts should be expressed as follows:

$$ {}^t\varepsilon_{ij} = {}^t\varepsilon_{ij}{}^E + {}^t\varepsilon_{ij}{}^{TH} + {}^t\varepsilon_{ij}{}^D + {}^t\varepsilon_{ij}{}^{TR} + {}^t\varepsilon_{ij}{}^P + {}^t\varepsilon_{ij}{}^C + {}^t\varepsilon_{ij}{}^{TP} \quad (6) $$

where ${}^t\varepsilon_{ij}{}^E$, ${}^t\varepsilon_{ij}{}^{TH}$, ${}^t\varepsilon_{ij}{}^D$, ${}^t\varepsilon_{ij}{}^{TR}$, ${}^t\varepsilon_{ij}{}^P$, ${}^t\varepsilon_{ij}{}^C$ and ${}^t\varepsilon_{ij}{}^{TP}$ are elastic, thermal, diffusion, phase transformation, plastic, creep, and transformation plastic strains, respectively [1]. The strains in the right-hand side of Eq. (6), except the elastic strain, are obtained by accumulating their momentary occurrences from the initial state to the time *t.* In his presentation, a sum of the thermal, diffusion and phase transformation strains is used as the expansion strain.

After describing strains, the author talks about a bending in water quenched cylinders with keyway. The bending in the cylinders can be explained only by axial strains and stress like springback in the beam, which is caused mainly by positive axial plastic strain occurring on the keyway side. It is also meaningful to know bending of steel plate made of austenitic stainless steel during one-sided nitriding, which is caused mainly by strain due to generation of expanded austenite and reduced by creep strain. The author adds a topic on curving of the Japanese sword as a related example.

Residual stress distributions in cylindrical steel specimens have been examined for a long time. The author explains the origin of inherent distribution shapes of residual stress and length changes in the specific experiments. Characteristics of distortion and residual stress in ring parts due to carburizing quenching and induction hardening have been known empirically. The author's presentation explains the origin of the characteristics by applying the approach. Also he describes how tensile stress generates in quench cracked parts [10].

Although there are other topics regarding the approach applied by the author, only a distortion in a steel plate specimen carburized on a single side and oil-quenched is described in detail as follows.

Distortion in a steel plate specimen carburized on a single side and oil-quenched. The bending in plates caused by carburizing quenching on one side is regarded as a meaningful problem in this field, because the simulated results by the two groups [11,12] was irreconcilable. Figure 11 shows the appearance of quenched plate specimens with different thickness, 100 mm in length and 20 mm in width [11]. Since a carbon concentration distribution in the 1 mm thickness plate is almost linear, it is possible to predict its bending curvature in furnace using properties depended on carbon concentration by hand calculation. This is also the reason why this problem is important.

Simulated longitudinal elastic, plastic, expansion, and total strains distribute in the 1 mm thickness plate along the distance from the anti-carburized surface during carburizing were obtained as shown in Fig. 12. Legends *A* corresponds to the beginning stage of carburizing in 930 °C, and *B* and *C* are the stages after keeping in carbon potential level 1.2 %C for 1.4 h and subsequently 0.9 %C for 1.0 h, respectively. Legends *D* and *E* show the stages after decreasing temperature from 930 to 870 °C and keeping the condition of the stage *D* for 0.5 h, respectively.

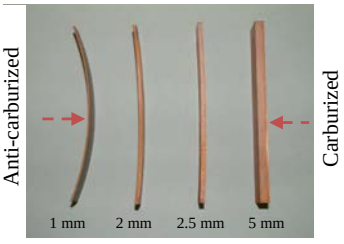

Fig. 11 Distortion in plates with different thickness

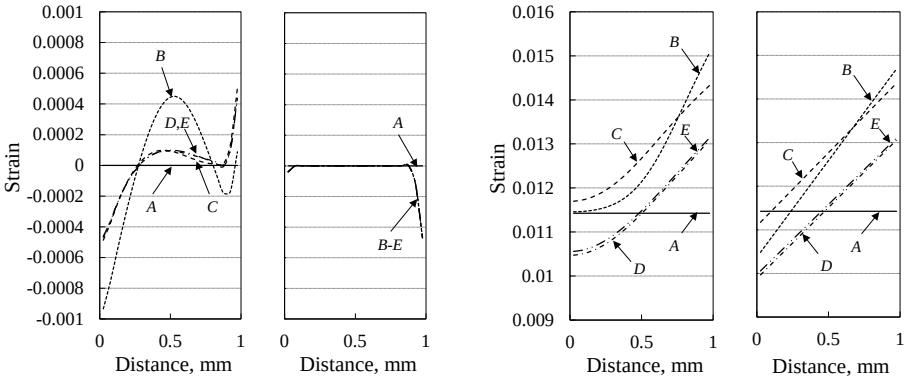

(a) Elastic (b) Plastic (c) Expansion (d) Total

Fig. 12 Simulated strain distributions in 1 mm thickness plate during carburizing

Distributions of expansion strain, which is the sum of thermal, diffusion and phase transformation

strains, change as shown in Fig. 12 (c). At the stage *A*, the expansion strain distribution becomes horizontal, and elastic and plastic strains have not been induced as shown in Figs. 12 (a) and (b), respectively. Also the total strain has a horizontal distribution as shown in Fig. 12 (d), which means no bending occurs at the stage *A*.

Until the stage *B*, carbon diffuses into the plate for 1.4 h at the 1.2 %C carbon potential, and then distribution of expansion strain depicts an upward trend as shown in Fig. 12(c) by diffusion strain. At the same time, elastic, plastic, and total strains appear as shown in Figs. 12 (a), (b), and (d), respectively. The linearity of total strain is derived from the hypothesis that cross sections remain plane in the plate. Then the nonlinearity in the expansion strain induces elastic and plastic strains under the strain equilibrium condition of Eq. (6). The upward linear distributions in total strain correspond to the similar trend of bending as shown in Fig. 11.

At the stage *C*, diffusion strain decreases in the region near the carburized surface, and increases in the inside of the plate by diffused carbon atoms as shown in Fig. 12 (c). Then elastic strain distribution turns flatter as shown in Fig. 12 (a). At the stage *D*, after decreasing temperature, expansion and total strain distributions move downward by keeping the shapes, as shown in Figs. 12 (c) and (d). Every strain changes less until the stage *E* which is at the end of carburizing.

Distribution shapes of diffusion strain at the stages *C* to *E* can be predicted by hand calculation when assuming a linear distribution of carbon concentration [11]. Using an empirical formula of austenite density dependent on temperature and carbon concentration, a diffusion strain difference when changing carbon concentration from 0.2%C to 0.85% C at 900°C can be obtained as 0.0032. This means that diffusion strain difference between the anti-carburized and carburized surfaces is 0.0032, which corresponds to the result in Fig. 12 (c) approximately.

Deflection at the midpoint of plate was calculated as 4.0 mm based on the simulated total strain distribution by a geometric relation of arc [11]. While Prantil et al. [12] showed the defection as 8 mm, which was obtained from their simulation for the experiment of the 1.3 mm thickness plate made of the steel which has a slightly different chemical composition from one in the Arimoto et al.'s study [11]. The large discrepancy between the two simulations is emphasized in the author's presentation.

During oil quenching after carburizing, temperature distributions in the 1 mm thickness plate decrease toward room temperature almost uniformly along the thickness. Meanwhile, martensite appears earlier near the anti-carburized surface since martensite-start temperature is higher therein by the lower carbon concentration.

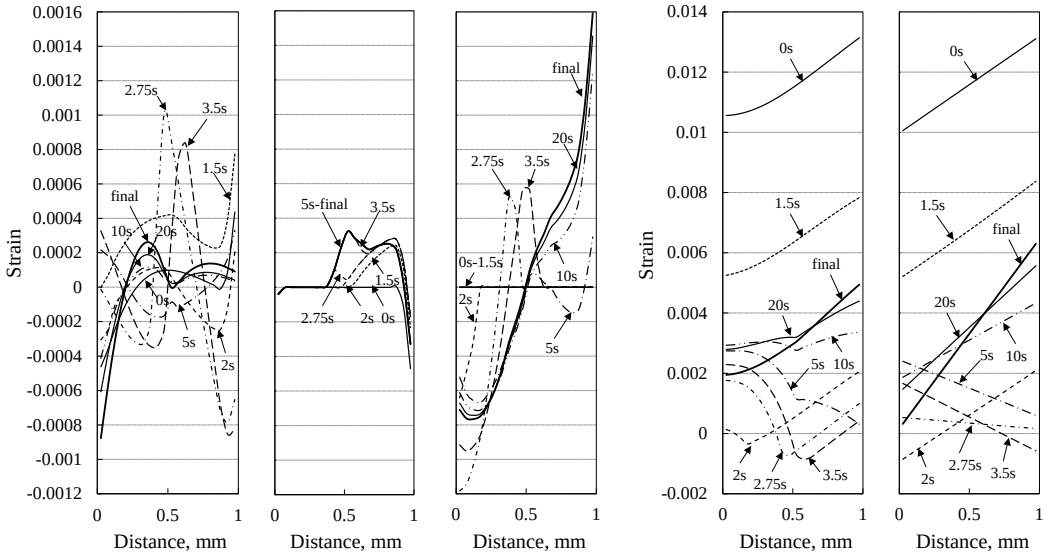

(a) Elastic (b) Plastic (c) Trans. plastic (d) Expansion (e) Total

Fig. 13 Simulated strain distributions in 1 mm thickness plate during oil quenching.

Changes of the strains during the oil quenching were obtained as shown in Fig. 13. Expansion strain distribution moves downward while keeping the shape until starting the martensitic transformation as shown in Fig. 13 (d). Martensite induced from the region near the anti-carburized surface contributes to increase expansion strain therein at 2 to 3.5 s. The delayed formation of martensite in the region near the carburized surface makes a downward trend in the expansion strain distribution at 5 s. When

achieving martensitic transformation almost in all regions, the shape trend of the expansion strain distribution becomes closer to the stage before cooling.

Total strain distributes linearly based on the hypothesis that cross sections remain plane in the bending plate as shown in Fig. 13 (e). Thus, elastic strain is induced due to nonlinearity occurred in the expansion strain distributions under the condition of Eq. (6). For example, significant elastic strain distribution caused at 1.5 s is due to this reason as shown in Fig. 13 (a), and also plastic strain occurs in the carburized region as shown in Fig. 13 (b). In addition, elastic strain distributes as large mountain and valley shapes at 2.75 and 3.5 s, which is induced by rapid transformed martensite only in the region near the anti-carburized surface. At 2.75 s, total strain distribution changes from upward to downward trends as shown in Fig. 13 (e). Finally, the same upward trend as the initial cooling stage appears at 10 s.

Transformation plastic strain is induced as shown in Fig. 13 (c) because of considerable stresses during the martensitic transformation. This strain appears near the anti-carburized surface from 2 s, while near the carburized surface from 5s. Induced transformation plastic strain contributes the steeper upward slope of the final total strain distribution, which agrees well with experimented bending curvature in the plate.

Summary

By analyzing the distribution stage of various strains from the simulated results, it is possible to explain the origin of distortion and residual stress generations. The author explains this simulated-strain based approach to novice engineers in a one-day course. The introduction part of the lecture uses unique conceptual diagrams to intuitively understand the essence of stress and strain, and also the spring back problem to connect easily to the approach in heat treatment.

Subsequently, by presenting applications of the approach, engineers understand that the origin of the distortion and residual stress are related to various strain conditions. Regardless of whether simulation is used or not, the applications of the approach to each problem make it easier to reach a solution in the real-world problems. Also contents of the one-day course will be effective to understand literatures on the subject.

References

[1] Arimoto, K., “Thermally-Processed Steels: Residual Stresses and Distortion”, In Encyclopedia of Iron, Steel, and Their Alloys, Taylor and Francis, New York, Published online: 13 Apr 2016; 3605-3633.

[2] Arimoto, K., “Learning about Stress and Strain for Real World Applications”, JSEE Annual Conference International Session Proceedings, 2018, pp. 59-64.

[3] Gere, J. M., “Mechanics of Materials”, 6th Ed., 2004, Thompson Publishing.

[4] Bowden, F. P. and Tabor, D., “Friction: an Introduction to Tribology”, Science Study Series No. 41, 1973, Anchor Press.

[5] Arimoto, K. Fredriksson, C., Silva, A., and Narahara, H., “Developing a Kit for Experiential Understanding of Elastic and Plastic Properties of Materials in Class”, JSEE Annual Conference International Session Proceedings, 2017, pp. 71-76.

[6] Wöhler, W., “Experiments to Determine the Forces Acting on Railway Car Axles and Its Strength”, Zeitschrift fur Bauwesen, 10, 1860, p. 583-616. (in German)

[7] https://www.youtube.com/watch?v=DaY47lKdgfI

[8] Gardiner, F. J., “The Springback of Metals”, Trans. ASME, Vol. 79, 1957, pp. 1-9.

[9] Ashby, M. F., “Materials Selection in Mechanical Design”, 5 th Ed., 2016, Elsevier.

[10] Arimoto, K., “Simulation of Steels Prone to Quench Cracking”, ASM Handbook, Volume 4D, Heat Treating of Irons and Steels, Dossett, J. and Totten, G. E. editors, 2014, pp. 44-57.

[11] Arimoto, K. “Studies on Distortions in a Steel Plate Specimen Carburised on a Single Side and Oil-quenched”, Int. J. Microstructure and Materials Properties, Vol. 10 (3/4), 2015, pp. 201-215.

[12] Prantil, V.C., Callabresi, M.L., Lathrop, J.F., Ramaswamy, G.S. and Lusk, M.T. “Simulating distortion and residual stresses in carburized thin strips”, ASME J. Eng. Mater. Tech., Vol. 125, 2003, pp.116–124.